Electronic structure and electron dynamics at an organic molecule/metal interface: interface states of tetra-*tert*-butyl-imine/Au(111)

2010 New J. Phys. 12 125022

(http://iopscience.iop.org/1367-2630/12/12/125022)

New Journal of Physics
The open-access journal for physics

Electronic structure and electron dynamics at an organic molecule/metal interface: interface states of tetra-*tert*-butyl-imine/Au(111)

Sebastian Hagen[1,2,4], Ying Luo[3], Rainer Haag[3], Martin Wolf[1,2] and Petra Tegeder[1,4]

[1] Freie Universität Berlin, Fachbereich Physik, Arnimallee 14, 14195 Berlin, Germany
[2] Department of Physical Chemistry, Fritz-Haber-Institut der MPG, Faradayweg 4-6, 14195 Berlin, Germany
[3] Institut für Chemie und Biochemie—Organische Chemie, Freie Universität Berlin, Takustrasse 3, D-14195 Berlin, Germany
E-mail: hagen@fhi-berlin.mpg.de and petra.tegeder@physik.fu-berlin.de

New Journal of Physics **12** (2010) 125022 (17pp)
Received 5 July 2010
Published 22 December 2010
Online at http://www.njp.org/
doi:10.1088/1367-2630/12/12/125022

Abstract. Time- and angle-resolved two-photon photoemission (2PPE) spectroscopies have been used to investigated the electronic structure, electron dynamics and localization at the interface between tetra-*tert*-butyl imine (TBI) and Au(111). At a TBI coverage of one monolayer (ML), the two highest occupied molecular orbitals, HOMO and HOMO-1, are observed at an energy of −1.9 and −2.6 eV below the Fermi level (E_F), respectively, and coincide with the d-band features of the Au substrate. In the unoccupied electronic structure, the lowest unoccupied molecular orbital (LUMO) has been observed at 1.6 eV with respect to E_F. In addition, two delocalized states that arise from the modified image potential at the TBI/metal interface have been identified. Their binding energies depend strongly on the adsorption structure of the TBI adlayer, which is coverage dependent in the submonolayer ($\leqslant$1 ML) regime. Thus the binding energy of the lower interface state (IS) shifts from 3.5 eV at 1.0 ML to 4.0 eV at 0.5 ML, which is accompanied by a pronounced decrease in its lifetime from 100 fs to below 10 fs. This is a result of differences in the wave function overlap with electronic states of the Au(111) substrate at different binding energies. This study shows that in order to fully understand the electronic structure of

[4] Authors to whom any correspondence should be addressed.

organic adsorbates at metal surfaces, not only adsorbate- and substrate-induced electronic states have to be considered but also ISs, which are the result of a potential formed by the interaction between the adsorbate and the substrate.

Contents

1. Introduction

The physical and chemical properties of molecules at surfaces play an important role in various fields, ranging from heterogeneous catalysis to nanoscale mechanics and organic optoelectronics [1]. While the properties of individual molecules can be modified in a controlled manner by chemical synthesis, their anchoring at surfaces can give rise to new functionalities, which may be used to design surfaces with specific properties [2]–[11]. The physical and chemical properties of such functionalized surfaces are determined by both the geometric structure (e.g. orientation with respect to the surface) and the electronic structure, which determines their optical, chemical and charge transport properties. Of special interest is a class of molecules that allow a transformation between two (or more) stable states with different physical properties as a result of an external stimulus. Such molecular switches at surfaces have attracted much interest because of their potential applications in nanotechnology, ranging from information storage and processing to adaptive surfaces [2, 3, 12, 13]. A major goal, relevant to the development of future applications, is to understand and control the structural changes in molecular switches at solid substrate surfaces. For this purpose, it is crucial to gain a detailed knowledge of the adsorption geometry (molecular orientation) and the electronic structure, i.e. the occupied and unoccupied electronic states (or band structure) of the molecules in contact with (metal) substrates.

Photochromic molecular switches, such as *N*-benzylideneaniline (also called imine; C_6H_5—CH═N—C_6H_6; see figure 1) and its derivatives, permit the control of the molecular geometry and functional properties with light [3, 14]. The photoinduced switching process observed in the liquid phase is based on a reversible *trans/cis*-isomerization. Thereby the photoisomerization is driven by an intramolecular electronic excitation. Imines are structurally similar and isoelectronic to azobenzene, which is the most thoroughly investigated molecular switch in solution [14]–[19]. Photoisomerization studies of molecular switches adsorbed on surfaces are also mostly carried out on azobenzene derivatives. Two different

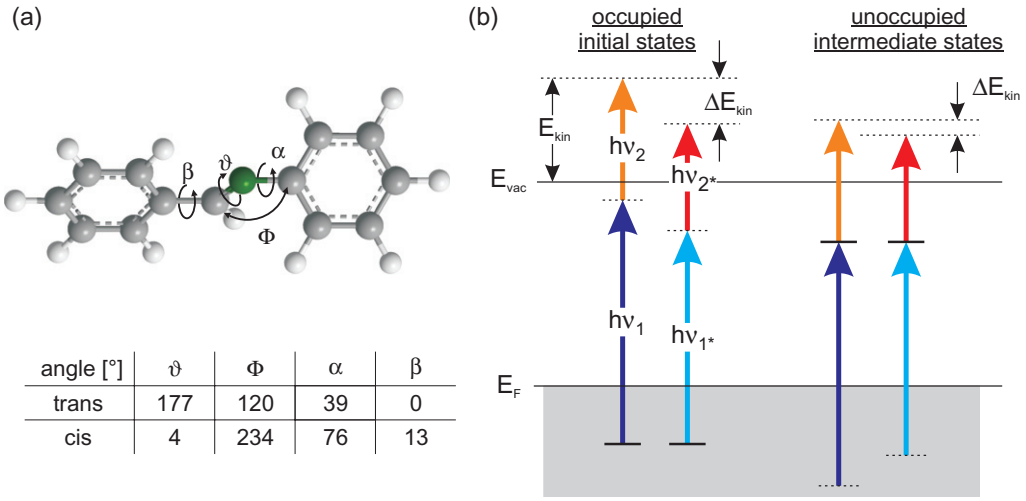

angle [°]	ϑ	Φ	α	β
trans	177	120	39	0
cis	4	234	76	13

Figure 1. (a) Ball and stick model of imine. The free molecule in solution can undergo a photoinduced *trans/cis*-isomerization. Here, the respective angles for *cis*- and *trans*-imine are given in the table (taken from [16]). (b) Pump–probe-energy scheme of 2PPE. Emitted electrons are analyzed with respect to their kinetic energy (E_{kin}). The corresponding spectra are a superposition of the signal from occupied and unoccupied states of the sample. To distinguish the respective contributions, the photon energy is varied. The kinetic energy of electrons from occupied initial states behaves according to $\Delta E_{\mathrm{kin}} = \Delta h\nu_1 + \Delta h\nu_2$. In the case of unoccupied intermediate states, E_{kin} is a function of the probe photon energy only. Depending on the energetic position of the intermediate state, we obtain either $\Delta E_{\mathrm{kin}} = \Delta h\nu_1$ or $\Delta E_{\mathrm{kin}} = \Delta h\nu_2$ (not shown here).

concepts concerning the connection of the molecular switches to the surface can be traced: (i) physisorbed or weakly chemisorbed systems (horizontal adsorption geometry) and (ii) via anchoring groups covalently attached to molecular switches incorporated into a self-assembled monolayer (vertical adsorption geometry). Using the latter concept, photoinduced switching has been demonstrated for several azobenzenes on gold surfaces (see for instance [20]–[27]). In the case of physisorbed molecules on metal surfaces (in direct contact with the metallic substrate), a photoinduced isomerization has so far been demonstrated only for a specifically designed azobenzene derivative, namely tetra-*tert*-butyl-azobenzene (TBA) adsorbed on Au(111) [28, 30]. Without doubt, the *trans/cis*-isomerization of TBA/Au(111) is the best-studied molecular switching process on a surface [28, 29], [31]–[36]. For TBA, it is believed that the bulky *tert*-butyl-groups lead to a decoupling of the functional azobenzene backbone from the metallic substrate, thus allowing the photoisomerization. Note that the photoinduced isomerization of bare azobenzene, i.e. the molecule bound to Au(111) without *tert*-butyl spacer, is suppressed presumably because of the stronger interaction with the metal substrate and corresponding differences in the electronic and geometric structures [30]. However, recent experimental studies using the normal incidence x-ray standing wave technique and large-scale density-functional theory calculations indicate a similar distance of the photochemically active diazo (—N═N—) bridge to the noble metal (Ag, Au) substrate for both the bare and *tert*-butyl functionalized azobenzene [37]–[39]. This demonstrates

that tuning the functionality of adsorbed molecules can be successful only if both the *geometric and the electronic structure* of the complete molecule–substrate complex are taken into account.

In general, the electronic structure of organic molecules adsorbed on metal or semiconducting surfaces, i.e. the energy level alignment at the interface, is of particular importance for the performance of e.g. optoelectronic devices. Bringing organic molecules in contact with a metallic substrate normally leads to a reduction of the HOMO–LUMO gap (HOMO refers to the highest occupied molecular orbital; LUMO refers to the lowest unoccupied molecular orbital) due to the image charge. The extent of the energy shift depends significantly on the strength of the molecule–substrate interaction. Using two-photon photoemission (2PPE) spectroscopy permits us to determine both the occupied and unoccupied electronic states (or band structure). Moreover, 2PPE can be carried out in a time-resolved fashion for the determination of charge carrier dynamics on a femtosecond time scale. Angle-resolved 2PPE measurements allow us to study electron localization/delocalization (dispersion) parallel to the surface [40]–[42]. 2PPE has been used in various adsorbate/substrate systems to study the adsorbate and image potential states (IPSs) as well as image-like unoccupied resonances [42]–[47]. The latter were first observed at the interfaces of thick rare-gas layers and metals by Rohleder *et al* [48, 49] and Güdde and Höfer [50]. These so-called buried interface states (ISs) have similar properties to IPSs, but are spatially located at the dielectric/metal interface, with energetic positions slightly above the vacuum level. They are explained by the superposition of atomic potentials of the adsorbate and the potential created by the image charge at the metal–adsorbate interface. A similar interfacial resonance has been proposed for an alkanethiolate self-assembled monolayer/Au(111) interface [51].

In this paper, we examined the electronic structure, electron dynamics and localization at the interface between 3,3′,5,5′-tetra-*tert*-butyl-imine (TBI) and Au(111) using time- and angle-resolved 2PPE. At a TBI coverage of one monolayer (ML), we find occupied electronic states at -1.95 and -2.6 eV with respect to the Fermi level (E_F), which we assign to HOMO and HOMO-1. In addition, LUMO is observed at 1.60 eV above E_F. Apart from these three TBI-derived electronic states, we identify two delocalized unoccupied electronic states that are located at the TBI/Au(111) interface. The two ISs originate from a modified image potential at the interface. Their binding energy strongly depends on the geometrical structure of TBI, which is coverage dependent. Due to a coverage-dependent binding energy in the low-coverage regime ($\leqslant 1$ ML), a pronounced change in the lifetime, from below 10 fs at 0.5 ML to ~ 100 fs at 1 ML, of the IS is observed.

Our results demonstrate that for a complete understanding of the electronic structure of organic molecules adsorbed on a metal surface, not only adsorbate- and substrate-derived electronic states have to be considered but also electronic states that are created at the molecule/metal interface. They are the result of a potential formed by the interaction between the adsorbate and the substrate.

2. Experimental details

For the 2PPE measurements, an ultrahigh vacuum chamber for photoemission spectroscopy and surface science techniques in combination with a tuneable femtosecond laser system was used.

The experiments were carried out under ultrahigh vacuum conditions (a base pressure of $p = 1 \times 10^{-10}$ mbar). The Au(111) crystal was mounted on a liquid helium cooled cryostat,

which in conjunction with resistive heating enables temperature control from 40 to 750 K. The crystal was cleaned by a standard procedure of Ar^+ sputtering ($V = 1.2$ kV) and annealing ($T = 800$ K). TBI molecules were dosed onto the Au(111) crystal using a home-built effusion cell held at 380 K. To determine the TBI coverage, thermal desorption spectroscopy (TDS) was used. In the TDS experiments, the substrate was resistively heated with a heating rate of 1 K s^{-1} and desorbing TBI was detected with a quadrupole mass spectrometer at the TBI-fragment mass of 190 amu (3,5-di-*tert*-butyl-phenyl ion). The integral of this signal is, in good approximation, directly proportional to the amount of desorbed molecules. The coverage is then given in multiples of a monolayer. The corresponding signal of the first ML can usually be distinguished within the spectra. Its binding energy, and thus the desorption temperature, generally differs from the binding energy of the subsequent layers. In the TDS of TBI, three desorption features (α_1–α_3) peaking around 290 K (α_1), 380 K (α_2) and 490 K (α_3) are observed, which are assigned to the desorption from the multilayer (α_1) and the first monolayer ($\alpha_2 + \alpha_3$), respectively. Thereby, the monolayer regime contains two desorption peaks (α_2, α_3), where α_2 represents the desorption of $\approx 50\%$ of the monolayer coverage.

To prepare TBI/Au(111) samples of defined coverages, we used two techniques. The first was based on the linear relationship between the dosing time and the resulting coverage. The second method was based on the variation in the substrate temperature. In the initial step, a high coverage sample is prepared and excess molecules are subsequently heated off. The temperature dependence of the coverage is obtained from the previously mentioned TDS experiments. A similar effect was achieved by raising the substrate temperature during the dosing process.

For the preparation of a monolayer, the sample was kept at $T = 300$ K, in order to avoid multilayer adsorption. In the case of multilayer preparation, the Au(111) is cooled to $T = 260$ K. Note that, for samples prepared at substrate temperatures $T < 200$ K, annealing effects were observed, i.e. changes in the photoemission signals as a function of substrate temperature. These effects are most likely attributed to a structural rearrangement of TBI, e.g. disorder/order effects. Consequently, all presented data originate from TBI-covered Au(111), which was annealed for at least 10 min at $T = 260$ K.

The femtosecond laser system consists of a Ti:sapphire oscillator in combination with a 300 kHz regenerative amplifier. It supplies pulses with a central wavelength ranging from 800 to 830 nm. The output is used to pump an optical parametrical amplifier, which yields photons with a tunable energy in the range from 1.7 to 2.7 eV. Through frequency doubling in a beta-barium borate (BBO) crystal, we can also achieve the photon energy range from 3.4 to 5.4 eV. After a thorough temporal compression, we obtain pulses with a duration of about 60 fs. These are focused onto the sample under an angle of 45° with respect to the surface normal.

For the 2PPE (pump–probe) experiments, we have to use photons with energies smaller than the work function of the adsorbate-covered Au(111) surface to avoid direct photoemission. In the pump–probe scheme (see figure 1(b)), the first photon ($h\nu_1$) is used to excite (pump) an electron from an initial occupied electronic state below the Fermi level (E_F) into either a real (e.g. the LUMO of the adsorbate) or a virtual unoccupied state below the vacuum level (E_{vac}). In a subsequent step, a second probe photon ($h\nu_2$) excites the electron above E_{vac}. To obtain information about the electronic structure, namely unoccupied and occupied electronic states, the kinetic energy distribution of the emitted electrons is recorded using a time-of-flight spectrometer.

The recorded 2PPE spectrum is the sum of electrons coming from occupied and unoccupied electronic states. In order to identify the respective contributions, one can take advantage of their

different photon energy dependences. As schematically shown in figure 1(b), the kinetic energy of electrons originating from occupied initial states (e.g. HOMO of the adsorbate) will scale with the change in the pump ($\Delta h\nu_1$) and probe ($\Delta h\nu_2$) photon energies, $\Delta E_{\mathrm{kin}} = \Delta h\nu_1 + \Delta h\nu_2$. In the case of an unoccupied electronic state (e.g. LUMO), only the probing photon influences the kinetic energy of the electron; hence $\Delta E_{\mathrm{kin}} = \Delta h\nu_2$. Note that this analysis is generally not applicable to transitions between bulk bands due to their strong perpendicular dispersion, but holds in the case of surface and adsorbate-derived states [52, 53].

Variation in the electron detection angle α with respect to the surface normal allows us to determine the electron momentum parallel to the surface $\hbar k_{\parallel}$ according to

$$\hbar k_{\parallel} = \sqrt{2m_{\mathrm{e}}E_{\mathrm{kin}}}\sin\alpha, \tag{1}$$

where m_{e} denotes the free electron mass and $k_{\parallel} = 0$ corresponds to electrons detected along the surface normal ($\alpha = 0$). For dispersion measurements, the vacuum levels of the sample and the spectrometer have to be balanced due to their different work functions by applying an appropriate bias voltage to the sample. Thereby, the deformation of the angular distribution of the emitted electrons by electric fields is minimized.

A powerful advantage of the 2PPE is its ability to monitor the decay of electrons (electron dynamics) from an unoccupied electronic state. Therefore, a temporal delay between the photons of the pump and the probe pulse is induced by changing the length of one of the beam paths. In the case of a trailing probe pulse, it can emit only electrons that at Δt have not yet decayed. Recording the respective 2PPE signal of unoccupied states as a function of the delay time yields the corresponding lifetime of the electronically excited states.

3. Results and discussions

Figure 2 shows a series of ultraviolet-photoemission spectra recorded at a photon energy of $h\nu = 6.1$ eV as a function of TBI coverage. These direct photoemission measurements allow us to determine the occupied electronic states of the TBI/Au(111) system. The spectrum of the bare Au(111) surface shows a sharp feature labeled as SS at a binding energy of $E = -0.48$ eV with respect to the Fermi level, which is associated with the Shockley surface state [54, 55]. The signal of the surface state decreases with increasing TBI coverage. Simultaneously, a smaller peak, SS′, appears at a binding energy of $E = -0.3$ eV. We assign this feature to the surface state of the adsorbate-covered Au(111) surface. Its binding energy and dispersion (not shown here) is consistent with results obtained from other adsorbate-covered Au surfaces [56]. At a TBI coverage of 1 ML, the surface state is completely quenched, whereas SS′ reaches its maximum intensity. The SS′ is also quenched as the coverage is further increased. The adsorption of TBI molecules leads to a reduction in the work function as can be directly witnessed in the broadening of the spectra when going from ≈ 0.15 to 1.1 ML. Thereby it is possible to probe deeper below the Fermi level. Consequently, we are able to resolve the Au sp-band observed at $E = -1.7$ eV. Note that due to a direct transition between the occupied and the unoccupied sp-band, this peak position does not reflect the actual binding energy, which is $E = -0.87$ eV (for detailed information see [57]). At a TBI coverage of 1.5 ML, a pronounced change in the photoemission spectrum occurs. The width of the spectrum decreases due to a drastic work function change.

A detailed picture of the coverage-dependent work function is given in figure 2(b). For this experiment, a multilayer of TBI/Au(111) has been prepared and is subsequently heated

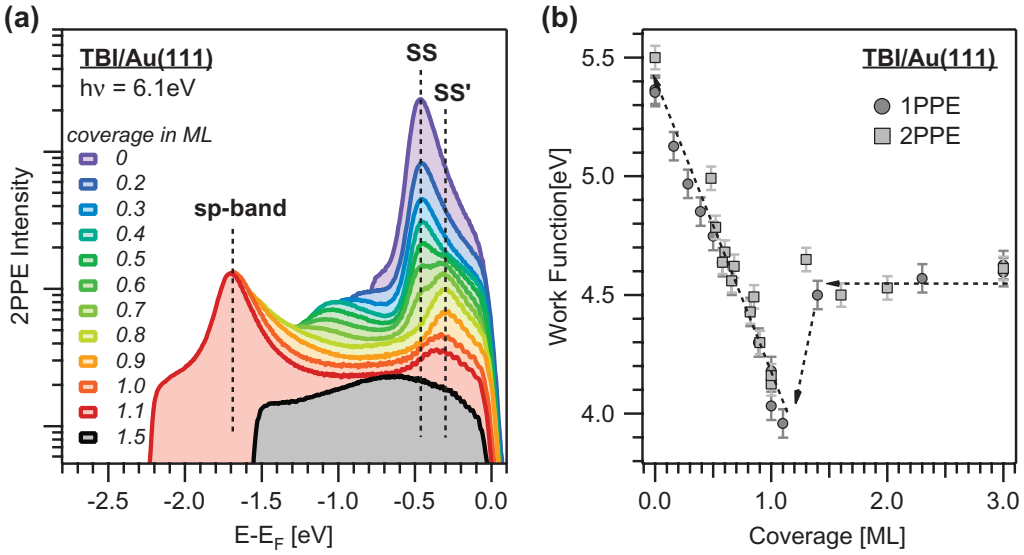

Figure 2. Coverage-dependent photoemission signal (a) and work function (b) of TBI/Au(111). For this experiment, a multilayer has been adsorbed on the surface at a substrate temperature of $T = 260$ K. The sample is subsequently heated to higher temperatures in order to partially desorb molecules and thereby reduce the coverage. (a) Direct photoemission signal mapping the occupied electronic structure of TBI/Au(111). The spectra are governed by the gold sp-band and two surface states (SS and SS′) of different binding energies. (b) Work function obtained from direct photoemission experiments at $h\nu = 6.1$ eV (circles) and various 2PPE measurements ($h\nu = 3.2$–4.5 eV). Both results show a large work function drop of $\Delta\Phi = 0.6$ eV on reduction of the coverage from 1.3 to 1.0 ML.

off. At 3 ML, we observe a work function of $\Phi = 4.5$ eV. It remains almost constant down to a coverage of 1.3 ML. In the region between 1.3 and 1.2 ML, Φ shows a sharp decrease of about 0.6 eV. From then onwards it continuously increases in an approximately linear fashion until all molecules are desorbed and the value of the clean Au(111) surface, $\Phi = 5.4$ eV, is reached. To verify the work function jump above the monolayer, additional data points obtained from 2PPE measurements have been included. They nicely fit into the data observed in the direct photoemission studies. The behavior of the work function as a function of TBI coverage, namely the drastic work function change of 600 meV in the vicinity of 1 ML, is quite unusual. We attribute this to a disorder/ordering effect of the TBI adlayers. High-resolution electron energy loss spectroscopy (HREELS) [58] performed by our group and near-edge x-ray absorption fine structure (NEXAFS) measurements [59] suggest that TBI undergoes a conformational change, i.e. a *trans*/*cis*-isomerization as a function of coverage in the low-coverage ($\leqslant 1$ ML) regime. Adsorption in the multilayer regime leads to unordered TBI molecules. At a coverage of 1 ML, TBI shows a bent (*cis*) configuration, while at coverages below 0.5 ML a planar (*trans*) form exists. Because of the different dipole moment of the *cis*- and *trans*-isomer, respectively, a huge change in the work function is observed in the submonolayer regime (a detailed discussion will follow in section 3.3). The calculated dipole moment of the unsubstituted imine is 1.43 and 2.60 D for the *trans*- and *cis*-imine, respectively [60]. Due to the coverage-dependent geometrical structure of TBI on Au(111), we will first focus on a Au(111) surface covered

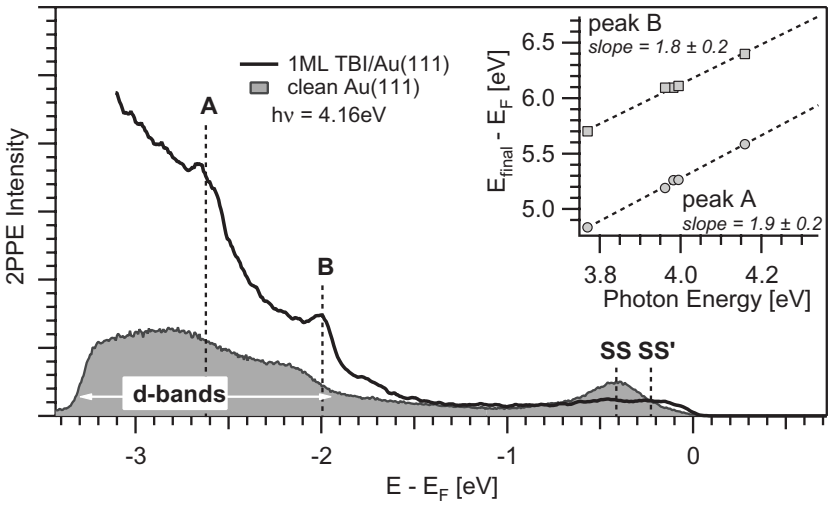

Figure 3. (a) One-color 2PPE spectrum of 1 ML TBI/Au(111). A comparison with the pure Au(111) signal (gray-shaded) reveals two molecule-induced states, labeled A and B, on top of the Au d-band contributions. The inset shows the final state energy of both peaks (energy of the emitted electrons with respect to E_F) as a function of photon energy. Both peaks scale with twice the photon energy, indicating that both peaks originate from occupied initial states in the 2PPE process.

with 1 ML TBI. This allows us to examine a defined adsorbate/substrate system, in which the molecules possess bent (*cis*)-configuration.

In the following, we present and discuss first the results obtained from the 2PPE on the electronic structure and the electron dynamics of 1 ML TBI adsorbed on the Au(111) surface. Thereafter, coverage-dependent measurements will be introduced to elucidate the origin of unoccupied electronic states observed in the photoemission spectra.

3.1. Electronic structure and electron dynamics at the tetra-tert-butyl imine (TBI)/Au(111) interface: one monolayer TBI

Figure 3 presents a one-color 2PPE spectrum of 1 ML TBI/Au(111) obtained with a photon energy of $h\nu = 4.16$ eV. In order to identify the contributions of the adsorbate, it is plotted together with a reference spectrum of the clean Au(111) surface. In the region close to the Fermi edge, we find the features of the two surface states SS and SS′ as observed in the direct photoemission experiment (see figure 2(a)). Two additional molecule-derived peaks labeled A and B appear in the spectral region of the gold d-bands ($E < 2$ eV) [61, 62]. To clarify the origin of both peaks, their energetic position within the spectra is measured as a function of the photon energy. The respective results are depicted in the inset of figure 3. According to the included linear fits, the energetic positions of both A and B scale with twice the photon energy, indicating that they arise from occupied initial states. Hence the respective electronic states are located at $E = -2.60$ eV (A) and $E = -1.95$ eV (B) below the Fermi level.

In order to provide access to unoccupied electronic states of TBI/Au(111), two-color 2PPE is used ($h\nu_2 = 2h\nu_1$). Figure 4(a) shows a spectrum of 1 ML TBI/Au(111) recorded at

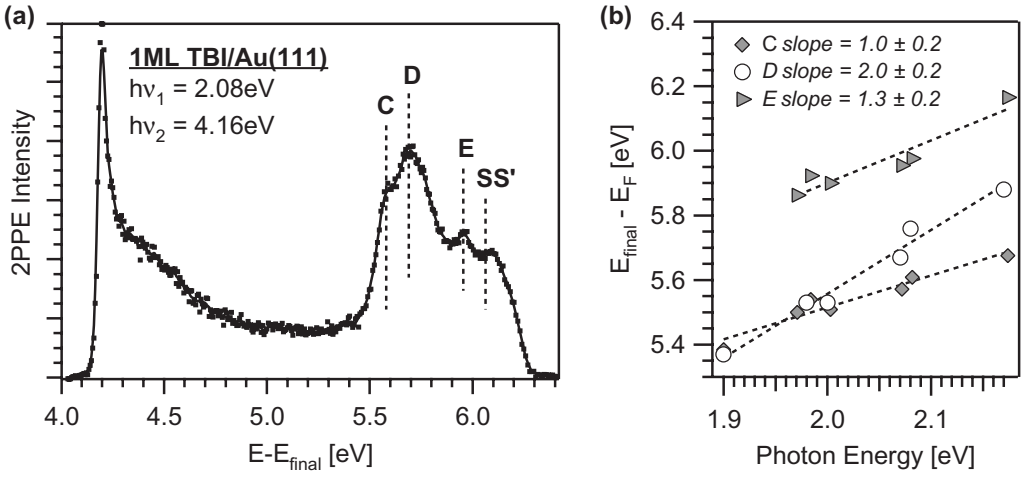

Figure 4. (a) Two-color 2PPE spectra of 1 ML TBI/Au(111) measured with 2.08 and 4.16 eV photons. (b) Photon energy dependence of peaks labeled C, D and E (see text).

photon energies of $h\nu_1 = 2.08$ eV and $h\nu_2 = 4.16$ eV. The spectrum is dominated by a broad feature close to the Fermi edge that contains contributions from four different, overlapping peaks. We identify the leftmost peak as the previously observed adsorbate-induced surface state SS′. To determine the energetic position of the remaining peaks, labeled C, D and E, their photon energy dependence is evaluated as a function of $h\nu_1$ (fundamental photons). As can be seen in figure 4(b), the fitting curves indicate that both peak C and peak E shift directly with $\Delta h\nu_1$, while D scales with $2\Delta h\nu_1$ (and hence with $h\nu_2$). Consequently, the corresponding electronic states are located above the Fermi level (unoccupied intermediate states). Thereby the unoccupied states labeled C and E are populated by the frequency-doubled photons ($h\nu_2$) and probed by $h\nu_1$; thus they are located at binding energies of $E = 3.5$ and 3.95 eV with respect to E_F. The peak labeled D, on the other hand, is pumped by the fundamental photons, resulting in a binding energy of $E = 1.60$ eV. Returning to the 2PPE spectra in figure 4(a), a strong exponential background can be observed, which we attribute to hot electrons from the substrate. This assignment is supported by the lifetime measurements presented below. On top of those hot electrons, the contributions of the gold d-bands can be observed as a small shoulder starting approximately 1.8 eV below the Fermi edge.

In the following, we determine the lifetime of the observed unoccupied electronic states using time-resolved 2PPE. Thereby a variable time delay, Δt, between the fundamental ($h\nu_1$) and the frequency-doubled laser pulses ($h\nu_2$) is introduced. The results for different Δt are displayed in a false color 2D representation, as shown for 1 ML TBI/Au(111) in figure 5. This shows the signal intensity as a function of the energy of the emitted electrons (vertical axis) and the pulse separation (horizontal axis). The trace in the right-hand side graph represents an energy spectrum taken at $\Delta t = 0$. It again exploits the four-peak structure previously observed in figure 4(a). To extract the lifetime of the corresponding states, the intensity of the signal is monitored at the respective energetic positions (dotted lines). The cross correlation traces for the energy region of peaks C and E are presented in the bottom panel. They are fitted assuming an exponential decay, taking into account the temporal shape of the laser pulses. The analysis yields a lifetime of $\tau = 110$ fs for the electronic state labeled C. For the state labeled E, on the

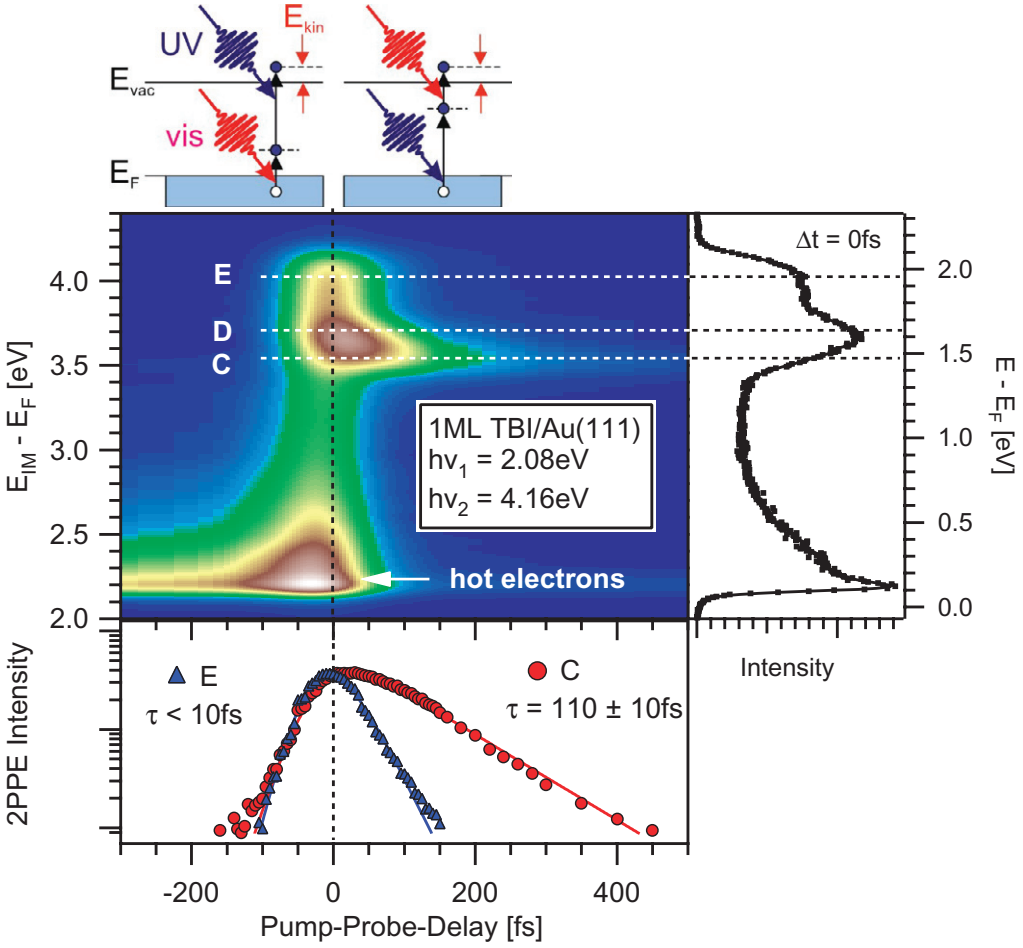

Figure 5. 2D spectra of a time-resolved two-color 2PPE measurement on 1 ML TBI/Au(111). The horizontal axis represents the temporal delay between the fundamental ($h\nu_1$) and the frequency-doubled ($h\nu_2$) pulses. At time zero, the pump–probe scheme is inverted, as shown in the sketch above. The intensity tail of peak C indicates a long lifetime of the corresponding $h\nu_2$ pumped state. Horizontally cutting the 2D plot at the respective intermediate state binding energy reveals an exponential decay (see the lower panel). It is fitted exponentially, taking into account the temporal shape of the two laser pulses. For 1 ML of TBI, a lifetime of $\tau = 110$ fs is obtained. The same procedure is applied for peak E. Its lifetime is below the resolution limit of 10 fs. To analyze peak D, we subtract the previously retrieved contributions from peak C. A fit of the remaining signal (not shown here) again yields a lifetime of $\tau < 10$ fs.

other hand, the lifetime is below the limit of the experimental resolution ($\tau < 10$ fs). To retrieve the decay rate of peak D, the previously extracted information is subtracted from the spectra. The remaining signal (not shown here) displays a symmetric (only folding of the laser pulses) behavior, indicating also a lifetime below the resolution limit. In the 2D plot, a second feature of extended lifetime can be found close to the vacuum edge. This signal originates from the previously mentioned hot electron distribution. It shows the typical decay rate of a couple of hundred femtoseconds.

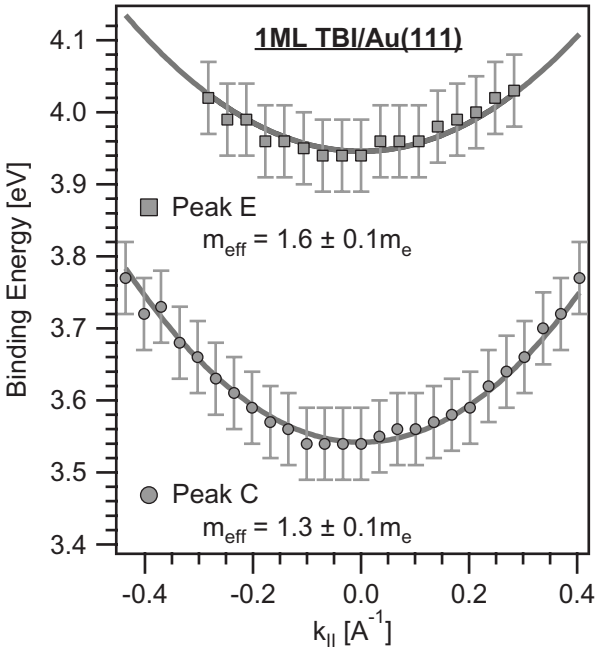

Figure 6. Angular-dependent 2PPE measurements from 1 ML TBI/Au(111), revealing the dispersion of the unoccupied states C and E. To obtain the momentum parallel to the surface ($k_{||}$), the sample is rotated in front of the analyzer (see equation (1)). The binding energy of peak C is evaluated at a pump–probe delay of $\Delta t = 120$ fs in order to separate it from the overlapping contributions of peak D.

To gain insights into the extent of electron delocalization/localization parallel to the surface, we performed dispersion measurements using angle-resolved 2PPE. In the case of the occupied states labeled A and B, the binding energy is independent of the detection angle (α) and thus of $k_{\parallel}$. The respective effective mass becomes infinity, indicating that the states are strongly localized. Due to the overlapping signal of the states labeled C and D, it is not possible to access their dispersion directly. However, at a monolayer coverage, we can extract information on peak C by conducting this experiment at pump–probe delays of $\Delta T > 60$ fs (see above). The corresponding values of the angle-dependent binding energy are shown in figure 6 together with the results for peak E. The dispersion curves can be described by a parabolic function $E_{\mathrm{kin}}(k_{\parallel}) = \hbar^2 k_{\parallel}^2 / 2m_{\mathrm{eff}} + E_{\mathrm{kin}}(k_{\parallel} = 0)$, where m_{eff} is the effective electron mass. The fits give an effective electron mass of $1.6 \pm 0.1 m_{\mathrm{e}}$ for peak E and $1.3 \pm 0.1 m_{\mathrm{e}}$ for peak C. Thus both states can be viewed as delocalized, namely free-electron-like within the surface plane.

3.2. Assignment of the electronic states of TBI/Au(111)

Figure 7 summarizes the energies of all electronic states observed at a coverage of 1 ML TBI on Au(111). The Fermi level of the Au(111) surface serves as a reference. The work function at the 1 ML coverage is $\Phi = 4.1$ eV. We relate the two molecule-derived occupied initial states labeled A and B to arise from ionization of HOMO and HOMO-1. They are located at $E = -2.0$ and -2.6 eV, respectively. This assignment is supported by the flat dispersion relation, which

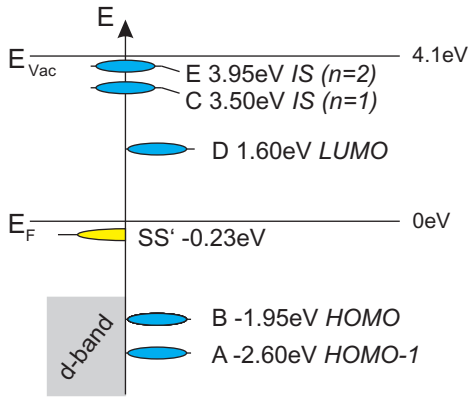

Figure 7. Schematic energy diagram for 1 ML TBI/Au(111). The peaks identified in the 2PPE spectra are plotted together with their binding energy with respect to the Fermi level of Au(111) and their assignment.

indicates the molecular character of both states. The unoccupied intermediate state labeled D shows an energetic position of 1.6 eV above E_F. We assign this peak to arise from photoemission of the LUMO of TBI. Here again, although the dispersion relation of the 2PPE peak cannot be fully resolved, the data indicate a localization of the electronic state. Consequently, we obtain a HOMO–LUMO gap of 3.6 eV. A similar value has been obtained from experiments on the isoelectronic system TBA/Au(111) [35]. Note that we do not observe a TBI coverage dependence on the energetic positions of the HOMO and LUMO levels in the coverage regime studied here (up to 3 ML).

In contrast to HOMO, HOMO-1 and LUMO, we find the unoccupied intermediate states labeled C and E to be delocalized. They show an energetic position of 3.5 and 3.95 eV above E_F, respectively, and thus a binding energy of 0.6 and 0.15 eV with respect to E_{vac}. The first and second IPSs (n = 1, 2) of the clean Au(111) surface are also located in this energy region. They possess a binding energy of 0.8 and 0.21 eV [63]. In order to understand the nature of these electronic states, we carried out coverage-dependent 2PPE measurements, since it is expected that IPSs are pinned to the vacuum level.

3.3. Coverage-dependent behavior of unoccupied electronic states: interface states

In the following, we will investigate the coverage-dependent characteristics, i.e. binding energy and lifetime of the unoccupied state labeled C and E. Figure 8(a) displays the binding energy of state C with respect to the Fermi level (circles) and with respect to the vacuum level (squares). Using E_F as a reference, we see that the binding energy is constant in the coverage regime from 1.0 to 3.0 ML TBI. However in the submonolayer range, the energy increases with decreasing coverage at least down to 0.5 ML of TBI/Au(111). Below 0.5 ML, the analysis of the peak position is prevented by the rising intensity of the Au(111) surface state feature, which coincides with the signal of peak C. The energetic position of state C with respect to E_{vac} is governed by the coverage-dependent work function. We observe a constant energetic position of 1 eV below E_{vac} in the coverage range from 1.3 to 3.0 ML. Between 1.0 and 1.3 ML, the binding energy decreases abruptly to approximately 0.6 eV, which is in agreement with the pronounced work function jump mentioned above (see figure 2(b)). With decreasing coverage, the binding energy

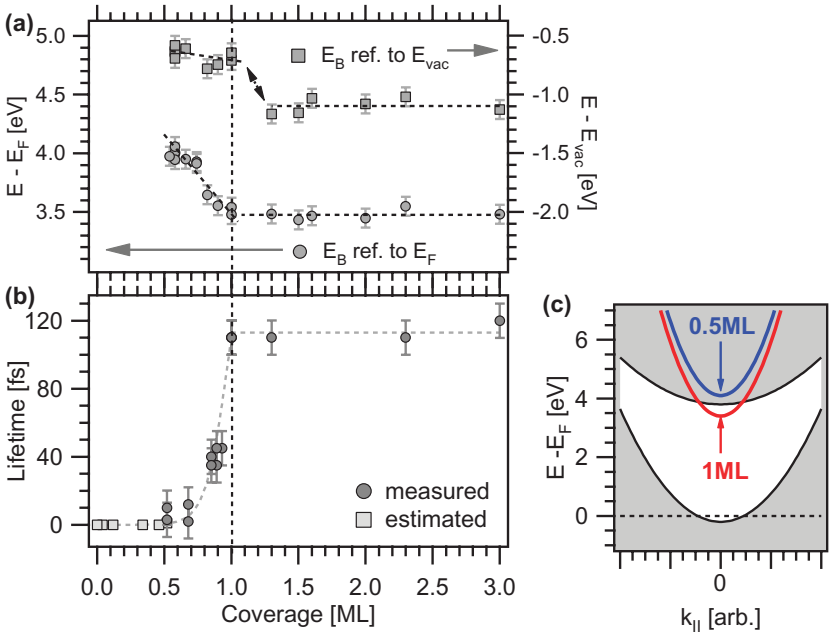

Figure 8. (a) Coverage-dependent energetic position of the intermediate state C with respect to the Fermi level (circles) and the vacuum level (squares). Due to the work function jump between 1.0 and 1.3 ML, the two traces show different behavior. (b) Coverage dependence of the state C lifetime. Down to 0.5 ML TBI/Au(111), the signal can be directly retrieved from the measurements. At lower coverages, C is hidden within the fast rinsing signal of the gold surface state. Since in the expected energy range of C no features can be found that indicate a lifetime, we assume that it remains below the resolution limit of 10 fs (squares). (c) Schematic depiction of the Au(111) band structure at the Γ-point. At coverages > 1.0 ML (red line), state C is located within the projected band gap (white area), whereas for low coverages (blue line) it overlaps with the unoccupied sp-band.

decreases slightly. Note that a similar coverage-dependent behavior of the binding energy is observed for the unoccupied state labeled E (data not shown here).

In summary, both states (C and E) show a constant binding energy with respect to E_F in the coverage regime from 1.0 to 3.0 ML, and they are clearly not pinned to the vacuum level of TBI/Au(111). The latter is especially obvious at the transition from 1.3 to 1.0 ML, where the work function experiences a sudden drop, whereas the energetic position of C and E remains constant. Correspondingly, the energy separation with respect to the vacuum level is increased by 400 meV. This strongly contradicts an IPS-like origin. Instead, we propose that both states are caused by a potential created at the molecule/metal interface. In this case, no effect of the layer thickness on the binding energy is expected and these ISs become independent of the work function. Due to the potential well, we assume that ISs form a Rydberg-like series akin to IPS. Therefore, we assign peak C to the $n = 1$ and peak E to the $n = 2$ interface state. In the case of the well-studied buried ISs of thick Ar films adsorbed on Cu(100) [48]–[50], which are structurally and electronically simpler compared to TBI/Au(111), the ISs originate

from the image potential of the metal, which is screened within the rare-gas layer. Thereby the attractive image potential of the metal within the rare-gas crystal represents a trap for electrons at the Ar/Cu interface. In the limit of an infinite layer thickness, an infinite Rydberg series with energies not aligned to the vacuum level (as for IPSs) but to the conduction band minimum of the adsorbate is formed. Due to the negative electron affinity of Ar, the ISs are located above E_{vac} in contrast to the ISs observed for TBI/Au(111), which possess an energetic position below E_{vac}. Note that TBI shows a negative electron affinity with the LUMO located at 1.6 eV above E_F corresponding to 2.5 eV below E_{vac} (for 1 ML TBI/Au(111)).

A further argument for the assignment of the state labeled C to be an interfacial state can be given by the coverage dependence of the lifetime. Figure 8(b) shows the lifetime (τ) of the electronically excited state C as a function of TBI coverage. Analogous to the behavior of the E_F referenced binding energy, τ is constant for coverages above the monolayer. In the submonolayer, it drops quickly from 110 fs at 1.0 ML to below the experimental resolution of 10 fs at 0.5 ML. At lower coverages, the time-resolved 2PPE signal does not show any signs of long-lived excited states. Hence, assuming that the energetic position of state C does not vary significantly, τ will remain below 10 fs in the range 0–0.5 ML (squares). Coming back to the nature of the electronic states C, for any unoccupied state the lifetime will be influenced by its coupling to the substrate. The coupling is predominantly determined by the binding energy, e.g. the energetic overlap with the substrate bulk bands, and the wave function penetration depth. At TBI coverages >1.0 ML the binding energy and the lifetime of state C are constant. This contradicts the behavior expected for an IPS, where due to the increasing layer thickness the wave function is pushed outwards and the coupling is thereby reduced [64]. Interfacial states, on the other hand, will remain unaffected by the adsorption of further molecules. In the submonolayer regime, the influence of the layer thickness is negligible. Here the coupling and thus the lifetime decrease can be attributed solely to the binding energy shift of interface state C. At 1 ML TBI/Au(111), it is located in the projected band gap, which extends to roughly 3.8 eV above the Fermi level [61]. With decreasing coverage, state C moves up in energy (see figure 8(c)), which is accompanied by an increasing overlap between the wave function and the unoccupied sp-band of the gold substrate. Consequently, more decay channels become available, reducing the lifetime. A similar effect on the lifetime of an excited state has been observed for the $n = 1$ IPS in the Xe/Cu(111) system by Hotzel *et al* [65]. In Cu(111), the $n = 1$ state is located near the top of the projected band gap of Cu(111). Adsorption of a monolayer Xe reduces the work function by 0.5 eV, which shifts the $n = 1$ IPS further away from the upper edge of the band gap. Accordingly, this results in an increase in the lifetime.

The energy shift of the IS as a function of TBI coverage in the submonolayer regime does not contradict our assignment. However, the origin of the observed binding energy change has to be discussed for further justification. A promising approach is the above-mentioned conformational change observed in HREELS [58] and NEXAFS [59] experiments. At 1 ML coverage, TBI shows a close-packed structure of bended *cis*-TBI. Upon desorption, a transition process occurs, which leads to flat-lying *trans*-TBI at 0.5 ML and below. In the intermediate regime from 0.5 to 1 ML, a mixture of both isomers will be present.

The conformational change of the TBI can be expected to influence the surface potential, presumably by a reorientation of the dipole moment. A similar effect has previously been observed for the isoelectronic TBA/Au(111) system [28]. The gradual change in the local surface potential, which is also influenced by the surrounding molecules, will then induce a continuous shift in the binding energy while going from the purely *cis* to the purely *trans*-TBI.

A second aspect of the conformational change is the increase in the work function. Again we refer to TBA/Au(111), where the light-induced *trans*/*cis*-isomerization has a similar effect on the work function [28]. Here the work function change can be directly related to the change in the dipole moment between the *trans*- and *cis*-isomer. For TBI/Au(111), the isomerization is induced by the desorption of molecules. Consequently, we have to consider two effects. The first effect is the earlier mentioned change of the dipole moment due to the *cis* to *trans* conformational change. The second effect is the reduction of the total number of molecules, which also contributes to the work function increase. This argument can well explain the unusual large Φ-shift of 1.3 eV when going from a bare substrate ($\Phi = 5.4$ eV) to a monolayer coverage ($\Phi = 4.1$ eV). At this point, we shall stress again the fact that in the coverage regime between 1.3 and 1 ML, the work function change is attributed to ordering effects.

4. Conclusions

In summary, 2PPE spectroscopy has been utilized to determine the electronic structure, electron dynamics and localization at the interface between TBI and Au(111). The 2PPE spectra show three TBI-derived photoemission peaks from which two are assigned to the HOMO and HOMO-1 and the third to the LUMO. The presence of the adsorbate induces a potential that hosts two electronic states located at the organic molecule/metal interface. This potential and therefore also the binding energies of the corresponding states are influenced by the conformation of the molecule, i.e. *cis*- or *trans*-TBI. TBI/Au(111) exploits a rather unusual coverage dependence of its work function, the binding energy and lifetime of the ISs. For coverages above 1.3 ML, the work function is raised by 0.5 eV with respect to the work function of 1 ML. The effect has been related to a disorder/order transition induced by desorption of TBI when going from 1.3 to 1.0 ML. In this coverage regime, the change in the work function had no influence on the IS binding energy. While an ordered monolayer of close-packed, bent (*cis*)-TBI is assumed, further desorption allows a gradual isomerization to the planar *trans*-isomer. At a coverage of 0.5 ML, all remaining molecules are expected to adopt a flat-lying *trans*-conformation. The coincidental change in the surface potential leads to an increase in the IS binding energy. Thereby IS is shifted from the band gap to an energetic region of the unoccupied gold sp-band. This drastically increases the wave function overlap with the bulk bands and thus significantly reduces the IS lifetime from 110 fs to below 10 fs.

Further experiments, including the determination of the electronic structure, electron dynamics and dispersion, of similar organic compounds adsorbed on noble metal surfaces are in progress. This may allow us to get a general picture of the existence and nature of interfacial states.

Acknowledgments

Funding by the Deutsche Forschungsgemeinschaft through SFB 658 ‘Elementary processes in molecular switches at surfaces’ is gratefully acknowledged.

References

[1] Waser R (ed) 2003 *Nanoelectronics and Information Technology* (Weinheim: Wiley)
[2] Balzani V, Credi A and Venturi M (ed) 2003 *Molecular Devices and Machines—A Journey into the Nanoworld* (Weinheim: Wiley)

[3] Feringa B L 2001 *Molecular Switches* (Weinheim: Wiley)
[4] Bryce M R, Petty M C and Bloor D 1995 *Molecular Electronics* (New York: Oxford University Press)
[5] Cuniberti G, Fagas F and Richter K (ed) 2005 *Introducing Molecular Electronics* (Berlin, Heidelberg: Springer)
[6] Irie M (ed) 1983 Photochromism: memories and switches *Chem. Rev.* **100** 1683
[7] Uchida K, Izumi N, Sukata S, Kojima Y, Nakamura S and Irie M 2006 *Angew. Chem. Int. Ed.* **45** 6470
[8] Rosario R, Gust D, Garcia A A, Hayes M, Taraci J L, Clement T, Dailey J W and Picraux S T 2004 *J. Phys. Chem.* B **108** 12640
[9] Katsonis N, Kudernac T, Walko M, van der Molen S J, van Wees B J and Feringa B L 2006 *Adv. Mater.* **18** 1397
[10] Joachim C, Gimzewski J K and Aviram A 2000 *Nature* **408** 541
[11] Katsonis N, Lubomska M, Pollard M M, Feringa B L and Rudolf P 2007 *Prog. Surf. Sci.* **82** 407
[12] Browne W R and Feringa B L 2006 *Nat. Nanotechnol* **1** 25
[13] Balzani V, Credi A and Venturi M 2008 *ChemPhysChem* **9** 202
[14] Padwa A 1977 *Chem. Rev.* **77** 37
[15] Gaenko A V, Devarajan A, Gagliardi L, Lindh R and Orlandi G 2007 *Theor. Chem. Acc.* **118** 271
[16] Bürgi H B and Dunitz J D 1970 *Helv. Chim. Acta* **53** 1747
[17] Tamai N and Miyasaka O H 2000 *Chem. Rev.* **100** 1875
[18] Rau H 2003 *Photochromism—Molecules and Systems* ed H Dürr and H Bouas-Laurent (Amsterdam: Elsevier)
[19] Fanghänel D, Timpe G and Orthman V 1990 *Organic Photochromes* ed A VEl'tsov (New York: Consultants Bureau)
[20] Pace G, Ferri V, Grave C, Elbing M, von Hänisch C, Zharnikov M, Mayor M, Rampi M A and Samorì P 2007 *Proc. Natl Acad. Sci.* **104** 9937
[21] Ferri V, Elbing M, Pace G, Dickey M D, Zharnikov M, Samorì P, Mayor M and Rampi M A 2008 *Angew. Chem. Int. Ed.* **47** 3407
[22] Yasuda S, Nakamura T, Matsumoto M and Shigekawa H 2003 *J. Am. Chem. Soc.* **125** 16430
[23] Kumar A S, Ye T, Takami T, Yu B-C, Flatt A K, Tour J M and Weiss P S 2008 *Nano Lett.* **8** 1644
[24] Ito M, Wei T X, Chen P-L, Akiyama H, Matsumoto M, Tamada K and Yamamoto Y 2005 *J. Mater. Chem.* **15** 478
[25] Callari F, Petralia S and Sortino S 2006 *Chem. Commun.* **9** 1009–11
[26] Cook M J, Nygrd A-M, Wang Z and Russell D A 2002 *Chem. Commun.* **22** 1056
[27] Wagner S, Leyssner F, Kördel C, Zarwell S, Schmidt R, Weinelt M, Rück-Braun K, Wolf M and Tegeder P 2009 *Phys. Chem. Chem. Phys.* **11** 6242–8
[28] Hagen S, Leyssner F, Nandi D, Wolf M and Tegeder P 2007 *Chem. Phys. Lett.* **444** 85
[29] Óvári L, Wolf M and Tegeder P 2007 *J. Phys. Chem.* C **111** 15370
[30] Comstock M J *et al* 2007 *Phys. Rev. Lett.* **99** 038301
[31] Hagen S, Kate P, Peters M V, Hecht S, Wolf M and Tegeder P 2008 *Appl. Phys.* A **93** 253
[32] Hagen S, Kate P, Leyssner F, Nandi D, Wolf M and Tegeder P 2008 *J. Chem. Phys.* **129** 164102
[33] Wolf M and Tegeder P 2009 *Surf. Sci.* **603** 1506
[34] Levy N, Comstock M, Cho J, Berbil-Bautista L, Kirakosian F L A, Poulsen D, Frechet J and Crommie M F 2009 *Nano Lett.* **99** 935
[35] Leyssner F, Hagen S, Óvri L, Dokic J, Saalfrank P, Peters M V, Hecht S, Klamroth T and Tegeder P 2010 *J. Phys. Chem.* C **114** 1231
[36] Schmidt R, Hagen S, Brete D, Carley R, Gahl C, Dokic J, Saalfrank P, Hecht S, Tegeder P and Weinelt M 2010 *Phys. Chem. Chem. Phys.* **12** 4488
[37] McNellis E R, Bronner C, Meyer J, Weinelt M, Tegeder P and Reuter K 2010 *Phys. Chem. Chem. Phys.* **12** 6404
[38] Mercurio G *et al* 2010 *Phys. Rev. Lett.* **104** 036102-1/-4
[39] McNellis E R, Mercurio G, Hagen S, Leyssner F, Meyer J, Soubatch S, Wolf M, Reuter K, Tegeder P and Tautz F S 2010 *Chem. Phys. Lett.* **499** 247

[40] Petek H and Ogawa S 1997 *Prog. Surf. Sci.* **56** 239
[41] Weinelt M 2002 *J. Phys.: Condens. Matter* **14** R1099
[42] Zhu X-Y 2004 *Surf. Sci. Rep.* **56** 1
[43] Schwalb C H, Sachs S, Marks M, Schöll A, Reinert F, Umbach E and Höfer U 2008 *Phys. Rev. Lett.* **101** 146801
[44] Lindstrom C D and Zhu X-Y 2006 *Chem. Rev.* **106** 4281
[45] Güdde J, Berthold W and Höfer U 2006 *Chem. Rev.* **106** 4261
[46] McNeill J D, Lingle R L, Jordan R E, Padowitz D F and Harris C B 1996 *J. Chem. Phys.* **105** 3883
[47] Harris C B, Ge N H, Lingle R L, McNeill J D and Wong C M 1997 *Annu. Rev. Phys. Chem.* **48** 711
[48] Rohleder M, Berthold W, Güdde J and Höfer U 2005 *Phys. Rev. Lett.* **95** 017401
[49] Rohleder M, Dunker K, Berthold W, Güdde J and Höfer U 2005 *New. J. Phys.* **7** 103
[50] Güdde J and Höfer U 2005 *Prog. Surf. Sci.* **80** 49
[51] Muntwiler M, Lindstrom C D and Zhu X-Y 2006 *J. Chem. Phys.* **124** 081104
[52] Plummer E W and Eberhardt W 1985 *Adv. Chem. Phys.* **49** 533
[53] Benning P J, Poirier D M, Ohno T R, Shen Y, Jost M B, Stepniak F, Kroll G H, Weaver J H, Fure J and Smalley R E 1992 *Phys. Rev.* B **45** 6899
[54] Kowalczyk P, Kozlowski W, Olejniczak W and Datta P K 2006 *Surf. Sci.* **600** 1604
[55] Hoesch M, Muntwiler M, Petrov V N, Hengsberger M, Patthey L, Shi M, Falub M, Greber T and Osterwalder J 2004 *Phys. Rev.* B **69** 241401
[56] Forster F, Bendounan A, Reinert F, Grigoryan V G and Springborg M 2007 *Surf. Sci.* **601** 5595
[57] Pontius N, Sametoglu V and Petek H 2005 *Phys. Rev.* B **72** 115105
[58] Koch M, Leyssner F and Tegeder P unpublished
[59] Weinelt M 2010 private communication, Max-Born-Institut, Berlin
[60] Dokí J 2010 *PhD Thesis* Univerität Potsdam http://opus.kobv.de/ubp/volltexte/2010/4179/
[61] Eckhart H, Fritsche L and Noffke J 1984 *J. Phys. F: Met. Phys.* **14** 97
[62] Courths R, Zimmer H-G, Goldmann A and Saalfeld H 1986 *Phys. Rev.* B **34** 3577
[63] Fauster T and Steinmann W 1995 *Electromagnetic Waves: Recent Developments in Research* ed P Halevi (Amsterdam: Elsevier)
[64] Hotzel A 2007 *Prog. Surf. Sci.* **87** 336
[65] Hotzel A, Moos G, Ishioka K, Wolf M and Ertl G 1999 *Appl. Phys.* B **68** 615